miércoles, 29 de abril de 2015
01:40 p.m.

1st Pan-American Congress on Computational Mechanics – PANACM 2015
XI Argentine Congress on Computational Mechanics – MECOM 2015
S. Idelsohn, V. Sonzogni, A. Coutinho, M. Cruchaga, A. Lew & M. Cerrolaza (Eds)

STRUCTURAL MODELS AND MECHANICAL TESTS IN THE DEVELOPMENT OF A COMMUNICATIONS SPACECRAFT

SANTIAGO TEMPONE*[1], MARCOS FRANCESCHINI
and EDUARDO N. DVORKIN*****

*INVAP S.E.
A. Cmte. Luis Piedrabuena 4950, R4803CPV, Bariloche, Río Negro, Argentina
stempone@invap.com.ar http://www.invap.com.ar/

** INVAP S.E.
A. Cmte. Luis Piedrabuena 4950, R4803CPV, Bariloche, Río Negro, Argentina
mfranceschini@invap.com.ar http://www.invap.com.ar/

*** SIM&TEC S.A.
Av. Pueyrredón 2130 5to.A, C1119ACR, Buenos Aires, Argentina
edvorkin@simytec.com http://www.simytec.com

Key words: spacecraft, finite elements.

Abstract. The objective of this paper is to discuss the development of the computational structural models that were used to check the structural strength and orbital alignment of the communications spacecraft ARSAT-1, designed and built by INVAP.

1 INTRODUCTION

The objective of this paper is to discuss the computational structural models that were developed to check the strength and orbital alignment of the communications spacecraft ARSAT-1, designed and built by INVAP S.E. at Bariloche, Argentina under ARSAT S.A. requirements.

The results of the computational models were used, by the satellite developers, to check the structural integrity of the spacecraft structure and its ability to withstand the in-orbit thermal cycles without losing the communication devices pointing. In more details, it can be assessed that the output of the computational models was used by the spacecraft developers for:

- verifying, at the structural design stage, that the structure had the required strength and stiffness and that its dynamic behavior was compatible with the dynamic environment of the launching vehicle and no undesirable resonances were to be encountered;
- planning the physical tests and establishing their limits in order to protect the integrity of the spacecraft, of its instrumentation and of the testing machines.

After the execution of the physical tests the simulation results and experimental determinations were confronted to validate the computational – experimental spacecraft qualification process.

Two consecutive physical models are normally used in the qualification of a spacecraft [1] [2]:

[1] The work presented in this paper was developed while at SIM&TEC S.A.

- first the structural test model (STM): it is a full size model in which all the structural components are assembled but the actual spacecraft equipment is replaced by syntonized dummies. The wiring and insulation blankets are not installed on this model;
- finally the protoflight test model (PFM): it is basically the actual spacecraft in its launching configuration. Due to the presence of the wiring and insulation blankets this physical model presents more damping under dynamic excitations than the structural one.

In this paper some of the tests and numerical models used to qualify the STM are discussed.

The physical tests are:

- dynamic tests: sinusoidal frequency dependent excitations (sine sweep test and acoustic excitations). These tests simulate the mechanical excitations of the spacecraft inside the launcher;
- vacuum thermal loading test (TVAC): used to simulate the thermal cycles that undergoes the spacecraft in orbit.

While the objective of the dynamic tests is to check the structural integrity of the spacecraft when inside the launching vehicle, the objective of the thermal test is to check the structural integrity and alignment preservation of the spacecraft in orbit under thermal cycles.

The spacecraft structure is assembled using threaded connections; hence, bolted joints are very important structural components; therefore, special attention was given to the simulation of their behavior: an ad hoc elastic-plastic model was used to incorporate into the model the possibility of the frictional joints slipping and the effect, on the communication devices pointing, of the slipping hysteresis that may be accumulated during the planned length of the spacecraft mission.

The effect of the shocks induced by the pyrotechnic devices used for the separation of the spacecraft from the launch vehicle and for the deployment of the solar panels and antennas were experimentally investigated using the STM and the PFM.

All the possible failure modes that can be encountered during the testing, launching and orbiting were investigated with the developed computational models and mechanical tests.

In the second section of this paper the main features of the spacecraft finite element model are discussed.

In the third section the determination of natural frequencies is discussed while in the fourth section the numerical simulation of quasi-static tests (sine burst) and the sine sweep tests are also discussed.

In the fifth section the experimental-numerical procedure used for analysing the results of the acoustic tests are presented.

Finally the sixth section deals with the thermo-elastic model and the threaded connection model.

The finite element analyses were conducted using the commercial code FEMAP with NX Nastran.

2 MAIN FEATURES OF THE SPACECRAFT FINITE ELEMENT MODEL

2.1 Discretization

In Figure 1 the finite element model of the STM is displayed.

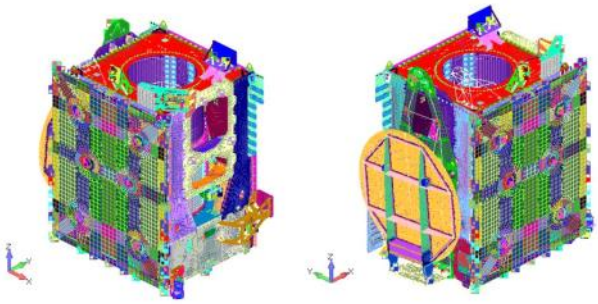

Figure 1. ARSAT-1 STM Finite Element model

The spacecraft panels are constructed using sandwich plates with an aluminum honeycomb core and facings made with aluminum in some cases and with carbon fiber laminates in other cases. In both cases the model is developed using laminate plate elements. In this kind of elements, in which the stiffness of the core is very different from the stiffness of the facings, a proper choice of the shear correction factors is of utmost importance to produce realistic results [3].

The function of the spacecraft handling adapter (SHA) is to fix the spacecraft to the shaker test table. The configuration of de shaker adapter is the same for Slip Table (SL) (X and Y horizontal directions) and Head Expander (HE) (Z vertical direction).

The SL adapter is composed by one intermediate plate, one base plate, one superior ring (SHA) and eight force-links as one of the options to be analyzed and sixteen force-links for the second option to be analyzed, as shown in Figure 2.

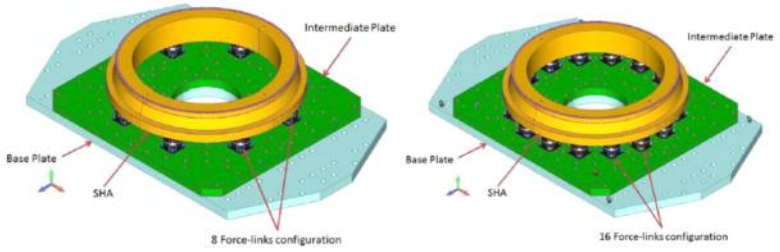

Figure 2. ARSAT-1 Slip Table (SL) and Spacecraft Handling Adapter (SHA) for 8 & 16 force links

The SHA is modeled using solid tetrahedral elements, while the plates are modeled with plate elements. Details of the mesh are displayed in Figure 3 and Figure 4.

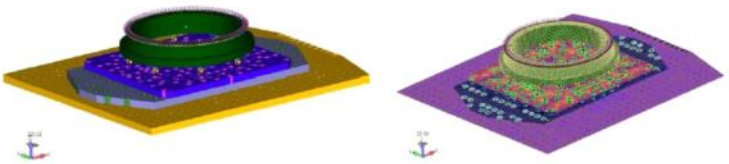

Figure 3. Eight - force-links adapter model with SL modeled

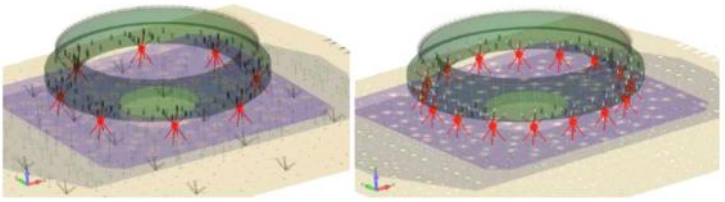

Figure 4. Eight and Sixteen force links configurations

The bolted connections are modeled using rigid links with a 6 d.o.f. spring elements (CBUSH elements) in series with it (Figure 5)

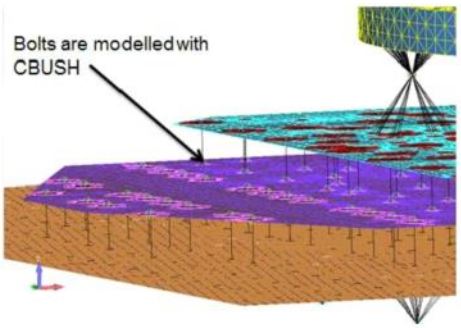

Figure 5. Bolted joints

The properties of CBUSH elements corresponding to bolted joints on the adapter were adjusted considering its stiffness. This adopted value was obtained through to a comparison between numerical

results from frequency analyses and results of the natural frequency test of the model performed at INVAP.

In Figure 6 the HE model is depicted.

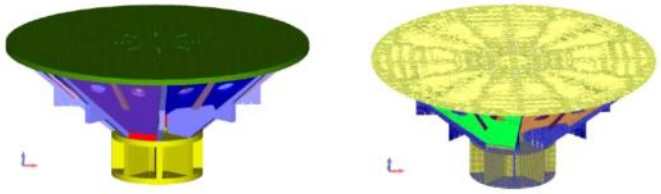

Figure 6. HE finite element model

In Figure 7 it is shown a force-link and a scheme of its model representation; the total mass of each force-link is simulated using two mass elements at the same geometrical location but using two different nodes: linked to the upper and lower rigid links respectively; a CBUSH, used to simulate the force-link manufacturer specified stiffness, links both masses.

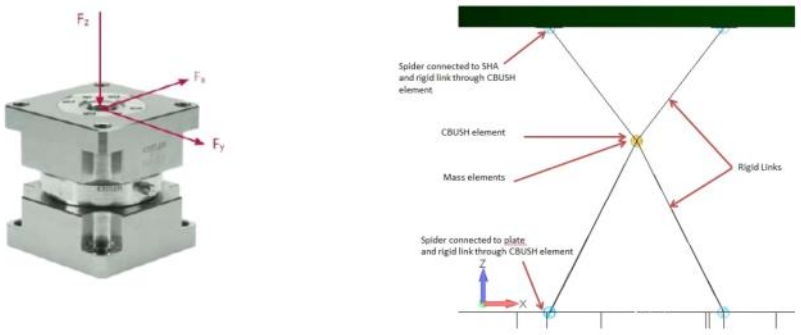

Figure 7. Force-link and its finite element model

The assembly of the SHA on the HE is shown in Figure 8.

Figure 8. Assembly SHA and HE

The total number of elements used in the different models is indicated in Table 1.

Table 1. Elements used in the developed models

	ARSAT-1 STM	8 F-L SHA+SL	16 F-L SHA+SL	8 F-L SHA+HE	16 F-L SHA+HE
Element Type	**# Elements**	**# Elements**	**# Elements**	**# Elements**	**# Elements**
Bar	1,243	1,243	1,243	1,243	1,243
Beam	1,146	1,146	1,146	1,146	1,146
CBUSH	3,284	3,540	3,612	3,540	3,612
DOF spring	4,911	4,911	4,911	4,911	4,911
Plate	138,218	265,334	265,334	385,167	385,167
Laminate	276,682	276,682	276,682	276,682	276,682
Solid	0	206,488	206,488	206,488	206,488
Mass	355	371	387	371	387
Rigid	9,778	11,326	11,374	11,395	11,443
TOTAL	**435,617**	**771,041**	**771,177**	**890,943**	**891,079**

2.2 Boundary conditions

For modeling the "Hard Mounted" condition all the 6 degrees of freedom of the nodes shown in Figure 9 were fixed.

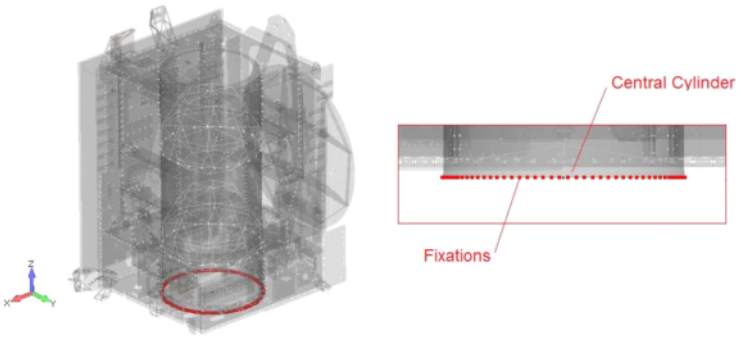

Figure 9. STM Hard Mounted boundary conditions

The SHA is fixed to the ST using 184 bolts as shown in Figure 10.

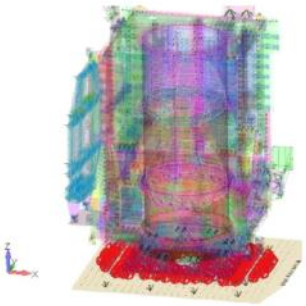

Figure 10. SHA fixation to the SL

The force-links (Figure 7) are fixed to the SHA and base plate as shown in Figure 11.

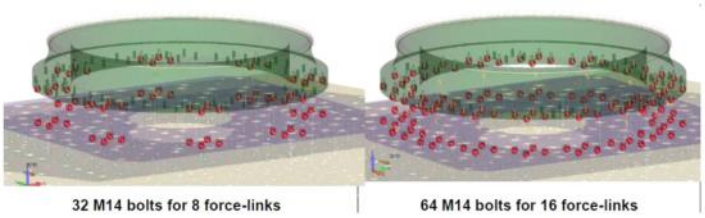

Figure 11. Force-links fixation bolts

When the HE is used, the fixations are shown in Figure 12.

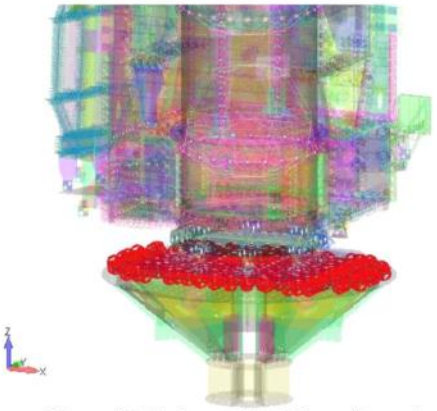

Figure 12. Bolts used in HE configuration

3 NATURAL FREQUENCIES

With the developed model, the natural frequencies in the interval [0, 150 Hz], of the hard mounted STM were determined, totalizing a number of 171 natural modes in the prescribed interval, Figure 13.

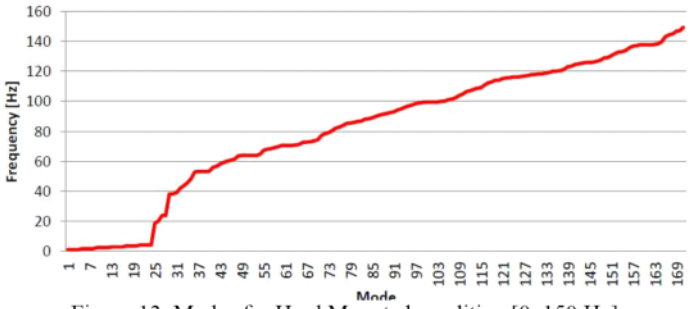

Figure 13. Modes for Hard Mounted condition [0, 150 Hz]

The first flexural modes and the axial mode are listed in Table 2.

Table 2. First natural frequencies for Hard Mounted condition

Mode	F (Hz)
First bending mode in the y-direction	18.74
First bending mode in the x-direction	20.13
First axial mode	61.37

The STM is mounted on the shaker using the SHA, the HE and the force-links. One of the objectives in the design of those intermediate parts is to minimize the difference between the natural frequencies of the STM as assembled on the shaker (Flexible configurations) and the STM Hard Mounted natural frequencies.

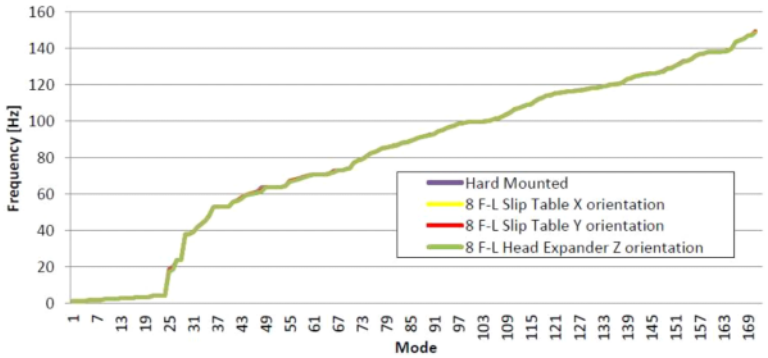

Figure 14. The 8 force-links condition

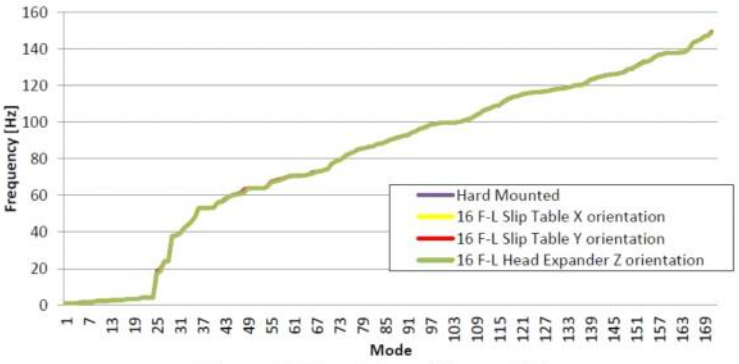

Figure 15. The 16 force-links condition

As it can be seen comparing Figure 14 and Figure 15 the change in natural frequencies introduced by the force-links is quite small.

In Figure16 and Figure 17, configurations corresponding to selected natural modes for the case of 8 force-links are shown for the STM assembled with the SL or HE.

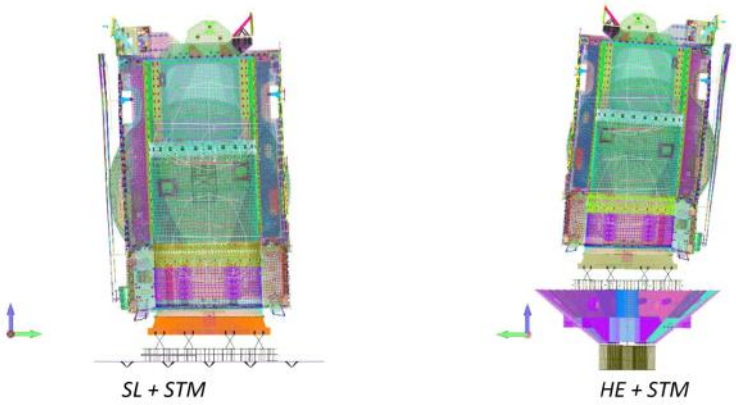

Figure 16. First flexural mode in Y-direction (8 force-links)

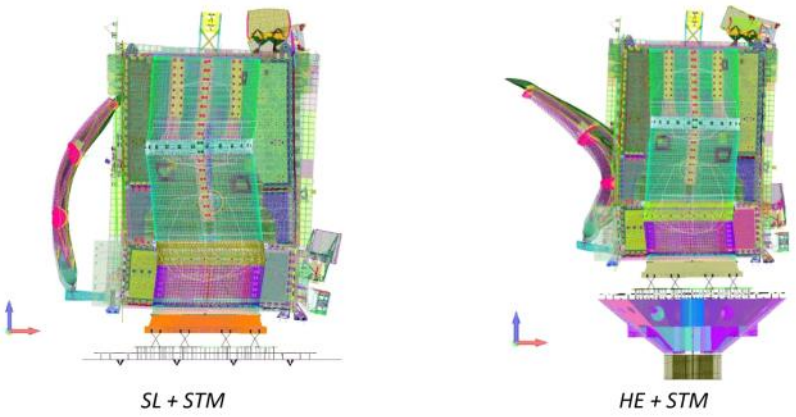

Figure 17. Second flexural mode in X-direction, counter-phase tanks (8 force links)

4 MODELING OF THE SINE BURST AND SINE SWEEP TESTS

4.1 The sine burst test

The sine burst test is a test, in which the ground acceleration is applied with the function [2],

$$g_{sb} = f(t)\, A_{sb} \sin(2\pi f_{sb}) \qquad (1)$$

where f(t) reaches its unit value after a number of cycles, remains equal to one from 5 to 10 cycles and then it descends to zero after a number of cycles. The frequency is $f_{sb} < \frac{f_n}{3}$, where f_n is the lowest natural frequency; hence, this test is modeled as a static test.

The accelerations considered in the static analysis are selected to induce the defined qualification loads at the separation plane.

Therefore the following three loading case accelerations are determined:

Table 3. Accelerations

Load case	X-acc [g]	Y-acc [g]	z-acc [g]
1	2.778	0	-1
2	0	2.778	-1
3	0	0	-8.49

The margins of safety in panels and bolts are determined using the mass loadings defined by Table 3.

4.2 The sine sweep test

A harmonic frequency response analysis is performed for 8 and 16 force-link configurations considering the adapter plus the STM plus the Slip Table / Head Expander. For each configuration, a

sine sweep in X, Y and Z direction is performed for the interval [0-100Hz]. An acceleration of **1g** is imposed in nodes that represent the Slip Table and Head Expander fixations to test machine.

Two structural damping coefficients are used: 2,5% for 0 to 50Hz and 1% for 51 to 100Hz.

The analyses are developed considering 8 and 16 force-links; to illustrate on the results in Figure 18 the results corresponding to the 8 force-links case presented.

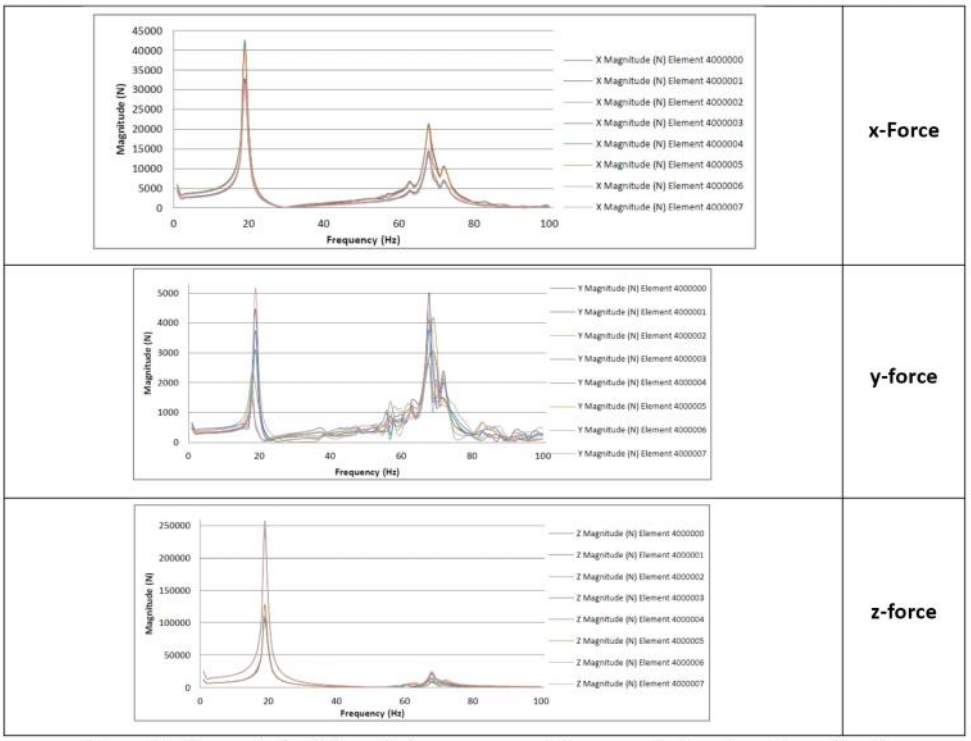

Figure 18. Forces in the 8 force-links arrangement for an excitation along the x-direction

With the results of the sine-sweep analyses the MS (margins of safety) of different structural elements like composite plates, threaded connections, etc. are calculated.

5 RANDOM AND ACOUSTIC EXCITATIONS

While the spacecraft is being transported by the launching vehicle towards the point of separation there are two important actions exerted by the launching vehicle on the satellite:

- random excitations introduced to the spacecraft through its base;
- acoustic excitations.

The random vibrations at the interface launcher-spacecraft are characterized using a PSD (Power Spectral density) distribution; in Figure 19 we present the one corresponding to the SOYUZ launching vehicle.

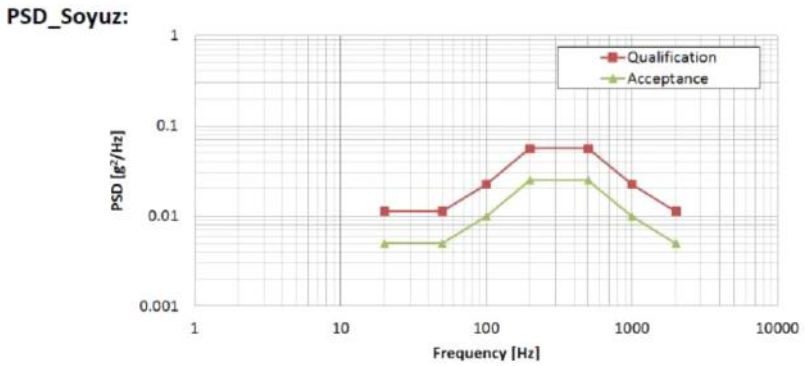

Figure 19. Random base vibrations *PSD_Launcher* (for qualification of components and for acceptance of components)

The methodology for verifying the different components is:

- define, either experimentally or with finite element models, the transfer function between the base and any component as a function of the frequency: $TF_{ii-jj}(f)$, where ii is the base vibration direction and jj is the direction of the component vibration;
- calculate for $jj = 1,2,3$ and for each frequency in the range [20Hz – 2,000Hz]

$$PSD\_Component_{jj} = PSD_{Launcher}\ [\max(TF_{11-jj}, TF_{22-jj}, TF_{33-jj})]^2 \quad (2)$$

- knowing the natural frequencies of the component (f_n) calculate the VRS (vibration response spectrum) for each natural frequency as shown in Figure 20 [4]. For this purpose use Miles equation in the form,

$$VRS_{component_{jj}}(f_n, \xi) = \frac{[1 + (2\xi\rho_i)^2]}{\left[\left(1 - \varrho_i^2\right)^2 + (2\xi\rho_i)^2\right]} PSD\_Component_{jj} \quad (3)$$

In the above equation $\varrho_i = {f_i}/{f_n}$ and ξ is the relative damping.

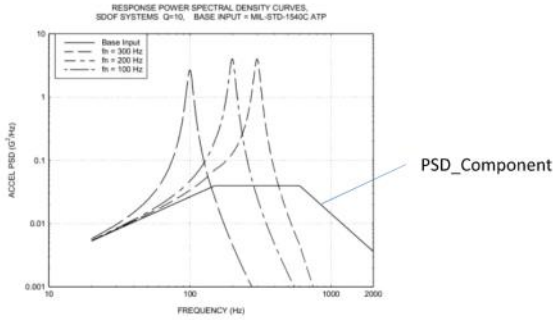

Figure 20. Determination of the VRS for each natural frequency of the component. PSD_component is determined with Eqn. (2)

- for each component natural frequency the RMS acceleration ($grms$) is calculated [4] as the area underneath the corresponding curve (blue area in the case in Figure 21);

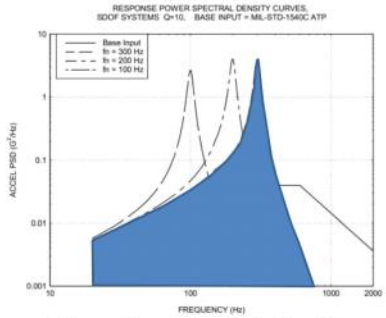

Figure 21. *grms* calculation [4]

The calculated grms is checked against the component allowable excitation.

In the ARIANE 5 launching vehicle, which is the one that was used for launching the ARSAT-1, it is specified that for less than 100 Hz the random environment is covered by the specified sine sweep environment and that the defined acoustic specification covers the excitations produced by random vibrations for frequencies above 100 Hz.

In Figure 22 it is shown the pressure level that was used in the DAF (direct acoustic field) test.

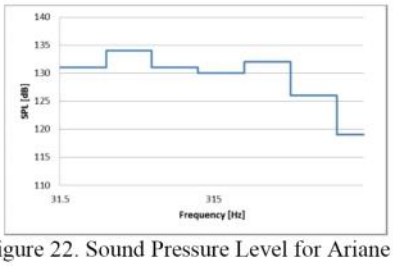

Figure 22. Sound Pressure Level for Ariane 5

In Figure 23 it is shown the arrangement for the PFM DAF test with the speakers surrounding the spacecraft and the control microphones indicated.

For assessing the effect of the acoustic field on the spacecraft components it is used as inputs the readings of the accelerometers located at the components basis (or quite close to them) in the DAF test.

The accelerometer readings are transformed into PSD at the base of each component.

The assessment methodology is based on the VRS methodology, using Eqn. (3) onwards.

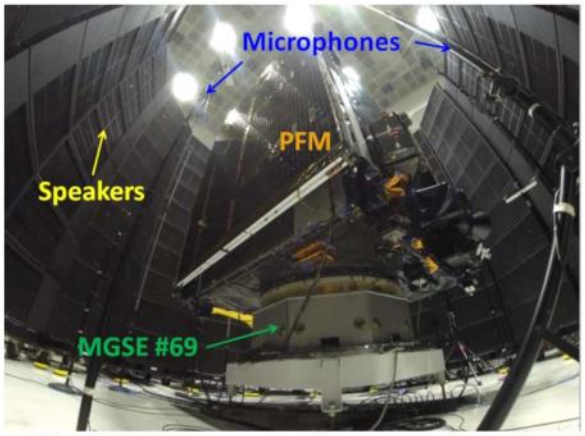

Figure 23. DAF test arrangement at CEATSA (Bariloche, Argentina)

6 THERMAL STRESSES

The calculation of thermal stresses proceeds from the determination of the satellite thermal maps for different positions along its orbit; a standard finite element procedure is used with a thermo-elastic material model, except for the threaded connections.

In Section 2 it was discussed the standard method for modeling bolted connections; however, for the thermo elastic analysis, since its results are fundamental for assessing the alignment preservation of the spacecraft in orbit under thermal cycles, it was considered necessary to introduce in the model:

- the possibility of connections slipping;
- the consideration of the hysteresis that may be introduced by the connections slipping.

In Figure 24 a bolted joint is represented. The nonlinear elastic CBUSH that models the bolted joint (Figure 25) includes and initial very stiff elastic part and then the bolted joint slip when the shear force Q is greater than the allowable shear force that can be transmitted by friction between the jointed surfaces. If the shear load is increased after this point, the bolt slides through the clearance. When the bolt gets in touch with the plates a stiffer part of the characteristic Load/Displacement curve represents the bearing between the bolt and the plates.

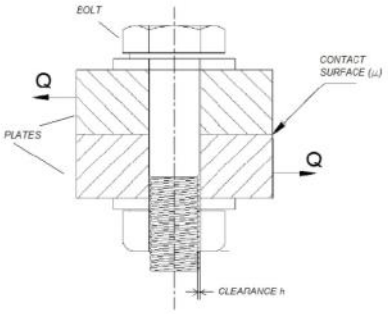

Figure 24. Bolted joint

Slippage occurs when the shear force exceeds the maximum allowable shear force, that is, when

$$Q > \mu P_o \qquad (3)$$

where,
μ: is the coefficient of static friction between the plates;
P_o: is the axial bolt preload.

The resulting nonlinear elastic CBUSH curve is displayed in Figure 25.

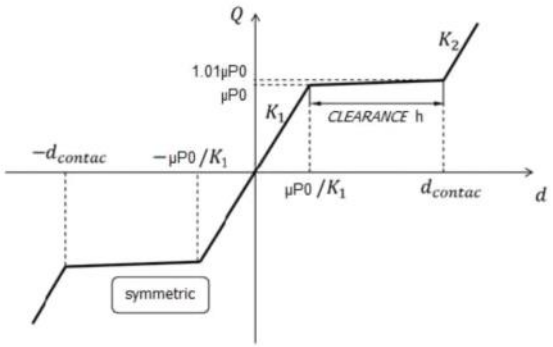

Figure 25. Nonlinear elastic CBUSH

The limitation of this connection model is that it cannot describe the hysteresis of the connections; hence an elasto plastic model was developed using elastic CBUHES and elasto-plastic rod elements as shown in Figure 26 and Figure 27.

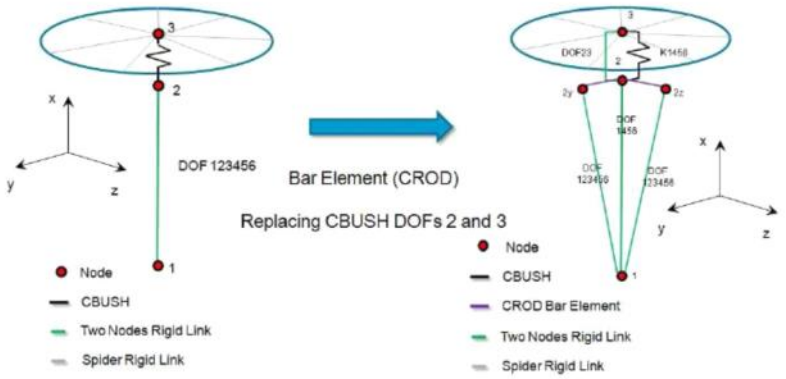

Figure 26. Evolution from the nonlinear elastic connection model to the elasto-plastic connection model

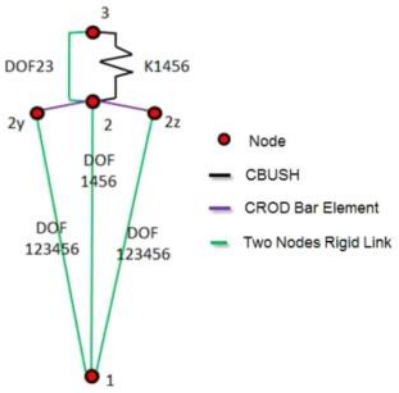

Figure 27. Details of the elasto-plastic connection model

The Load / Displacement characteristic of this model is represented in Figure 28.

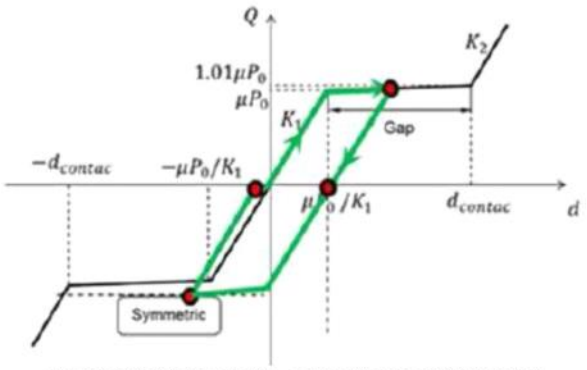

Figure 28. Elasto-plastic connection model behavior

Using this model it was shown that the hysteresis of the bolted connections is negligible and the more simple nonlinear elastic model can be reliably used.

7 CONCLUSIONS

A procedure for the development of finite element models of a spacecraft was discussed. The procedure was used by SIM&TEC and INVAP for the modeling of the ARSAT-1 communications satellite.

Acknowledgement

The authorization of ARSAT S.A. INVAP S.E. for the publication of this paper is gratefully acknowledged.

REFERENCES

[1] J. Wijker, Mechanical Vibrations in Spacecraft Design, Springer, 2004.

[2] J. Wijker, Spacecraft Structures, Springer, 2010.

[3] O. Guillermin, M. Kojic y K.-J. Bathe, «Linear and nonlinear analysis of composite shells,» de *Proceedings of STRUCOME 90*, 1990.

[4] T. Irvine, «An introduction to the vibration response spectrum (Rev. D),» www.vibrationdata.com, 2009.